

The Relationship between Double-Diffusive Intrusions and Staircases in the Arctic Ocean

YANA BEBIEVA AND MARY-LOUISE TIMMERMANS

Department of Geology and Geophysics, Yale University, New Haven, Connecticut

(Manuscript received 6 December 2016, in final form 31 January 2017)

ABSTRACT

The origin of double-diffusive staircases in the Arctic Ocean is investigated for the particular background setting in which both temperature and salinity increase with depth. Motivated by observations that show the coexistence of thermohaline intrusions and double-diffusive staircases, a linear stability analysis is performed on the governing equations to determine the conditions under which staircases form. It is shown that a double-diffusive staircase can result from interleaving motions if the observed bulk vertical density ratio is below a critical vertical density ratio estimated for particular lateral and vertical background temperature and salinity gradients. Vertical background temperature and salinity gradients dominate over horizontal gradients in determining whether staircases form, with the linear theory indicating that perturbations to stronger vertical temperature gradients are more likely to give rise to a staircase. Examination of Arctic Ocean temperature and salinity measurements indicates that observations are consistent with the theory for reasonable estimates of eddy diffusivity and viscosity.

1. Introduction

The Arctic Ocean has a strong halocline and deeper water layers that are warmer than those at the surface in contact with sea ice cover (e.g., Aagaard et al. 1981). Understanding the mechanisms and magnitude of upward fluxes of deep-ocean heat is essential to predictions of Arctic sea ice and climate (e.g., Maykut and Untersteiner 1971; Wettlaufer 1991; Perovich et al. 2008; Carmack et al. 2015; Timmermans 2015). Relatively cold and fresh surface waters, originating from net precipitation, river runoff, inflows from the Pacific Ocean, and seasonal sea ice melt, occupy the upper ~150–200-m water column of the Arctic Ocean's Canada Basin (e.g., Steele et al. 2008; Timmermans et al. 2014). Below these upper layers lie relatively warm and salty waters associated with Atlantic Water (AW) inflows, centered around 400-m depth in the Canada Basin, with lateral temperature gradients indicating a general cooling moving east from the warm core of the AW layer on the western side of the basin (Fig. 1a).

The basic vertical stratification, in which temperature and salinity both increase with depth, provides conditions amenable to double-diffusive instability, believed to be a key physical process generating thermohaline intrusions

and staircases in the Arctic Ocean. Throughout much of the central Arctic Ocean Basins, heat transfer from the AW layer is via double-diffusive convection (e.g., Melling et al. 1984; Padman and Dillon 1987, 1988; Timmermans et al. 2008; Polyakov et al. 2012; Sirevaag and Fer 2012; Guthrie et al. 2015). Two types of double-diffusive convection can arise in a stably stratified ocean: the case when both temperature T and salinity S increase with depth is referred to as diffusive convection [DC; an overview is given by Kelley et al. (2003)], while the case when both temperature and salinity decrease with depth is referred to as the salt-finger (SF) regime [for overviews, see, e.g., Kunze (2003) and Schmitt (2003)]. These stratifications may be characterized by a density ratio, which we define here as $\overline{R}_\rho = \beta \overline{S}_z / \alpha \overline{T}_z$, where the subscript z denotes the vertical gradient, and $\beta = (1/\rho_0)(\partial\rho/\partial S)_{T,p}$ and $\alpha = -(1/\rho_0)(\partial\rho/\partial T)_{S,p}$ (where ρ_0 is a reference density) are the saline contraction and thermal expansion coefficients, respectively. The overlines indicate a bulk gradient, taken to be linear over some specified depth range.

At the top boundary of the AW layer in the Canada Basin, a prevalent DC staircase is characterized by a sequence of mixed layers of thickness on the order of several meters separated by sharp gradients in temperature and salinity (e.g., Neal et al. 1969; Padman and Dillon 1987; Timmermans et al. 2008; Figs. 1b,c). Thermohaline intrusions, characterized by DC and SF regions alternating in depth, are often found underlying the staircase

Corresponding author e-mail: Yana Bebieva, yana.bebieva@yale.edu

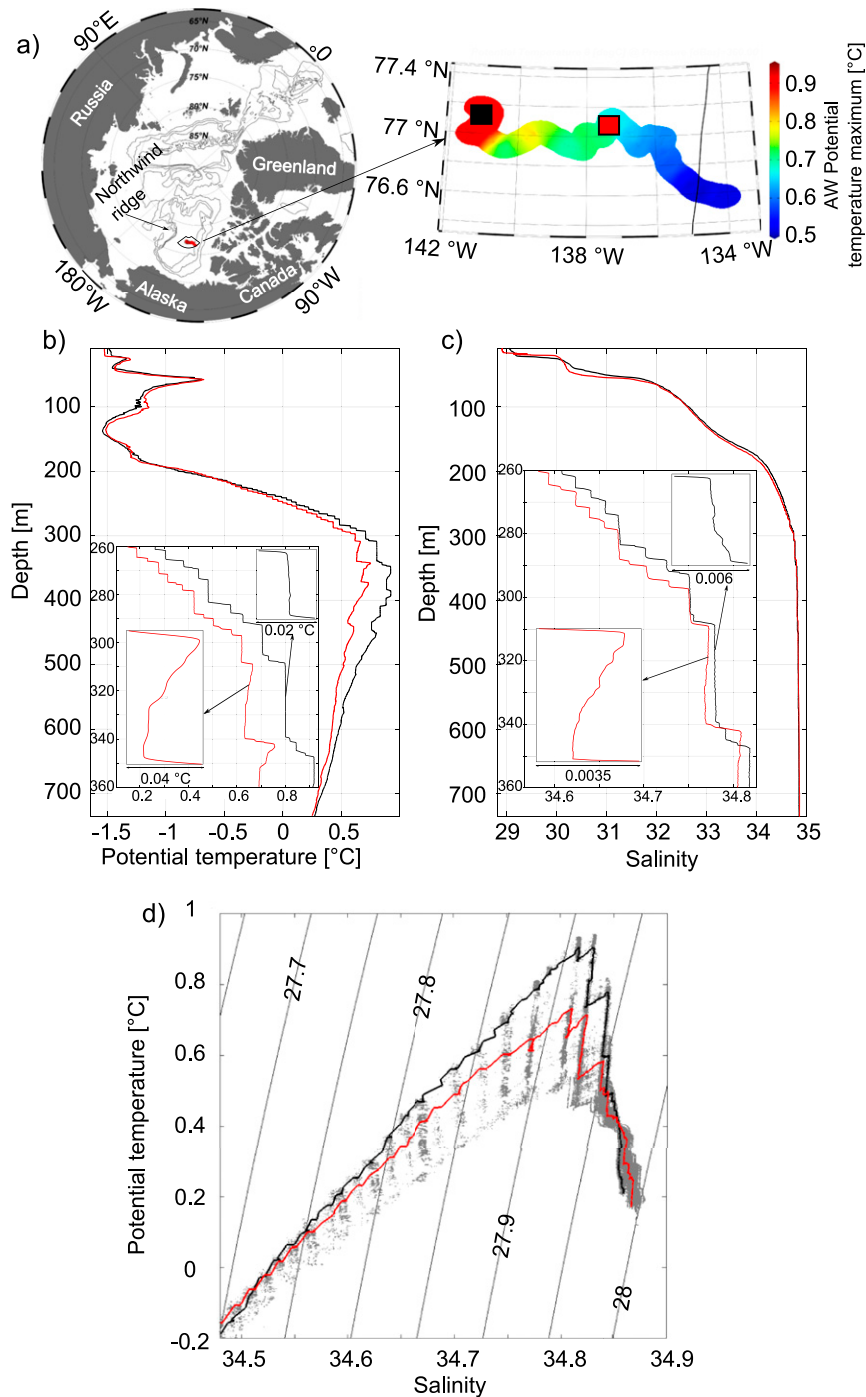


FIG. 1. (a) Map showing locations of ITP 2 profiles over the course of its drift; colors indicate the AW potential temperature maximum (°C). (b) Potential temperature (°C, referenced to the surface) and (c) salinity profiles measured on 22 Aug 2004 (black lines) and 3 Sep 2004 (red lines); locations where both profiles were sampled are marked by squares with corresponding colors on the map in (a). The expanded scales highlight double-diffusive structures. (d) Potential temperature and salinity values measured by ITP 2 between ~200- and ~750-m depth (gray dots, all profiles are shown); black and red lines correspond to the profiles shown in the same colors in (b) and (c). Thin black contours indicate potential density anomaly (kg m^{-3}) referenced to the surface.

(e.g., Carmack et al. 1998; Merryfield 2002; Woodgate et al. 2007). Intrusions are believed to be associated with lateral (in addition to vertical) gradients in temperature and salinity and are driven partly by vertical buoyancy flux divergences [overviews of thermohaline intrusions are given by Ruddick and Kerr (2003) and Ruddick and Richards (2003)].

Understanding the observed vertical temperature–salinity structure (whether staircases or intrusions) and associated vertical and lateral heat fluxes from the AW layer requires knowledge of the origins of these features and their relationship to each other (see Kelley 2001). Extensive efforts have been made to explain staircase and intrusion origins and evolution with respect to the SF configuration of double diffusion. There exist around six theories for the origin of SF staircases, as reviewed by Radko (2013). One of these theories is that interleaving motions can develop into a staircase (Merryfield 2000). The idea relies on the presence of lateral temperature and salinity gradients and builds on previous studies that invoke a standard parametric flux model (Walsh and Ruddick 1995, 2000). This model was first introduced by Stern (1967), who delineated three separate scales of motion: small, to describe double-diffusive processes on centimeter to meter scales; medium, to describe the scales of interleaving (order tens of meters vertically and kilometer scales laterally); and large, to characterize the background state (the full thickness of the double-diffusive region in depth and tens to hundreds of kilometers laterally). The main assumption here is that medium-scale dynamics are qualitatively similar to small-scale dynamics and that the effects of double diffusion can be parameterized in terms of eddy diffusivities. Merryfield (2000) applied this formalism in his calculations showing that interleaving motions evolve into SF staircases when the density ratio of the background (SF stratified) state is below a certain value (i.e., there exists a critical density ratio that delineates the boundary between staircase and intrusion formation).

Very little has been done with respect to analysis of staircase origins in the DC-stratified setting. The purpose of this study is to address the relationships between and origins of DC staircases and intrusions, with consideration of those in the Arctic Ocean. Temperature and salinity profiles from the Canada Basin show the presence of both staircases and intrusions shallower than the AW temperature maximum. Often the exact structure differs from region to region; for example, in some regions, only a staircase is observed in the upper part of the AW layer (Figs. 1b,c; black line), while in others, intrusions are observed instead (Figs. 1b,c; red line). Motivated by these observations that show staircases and intrusions coexisting and evolving, we assess the main factors that may determine whether staircases or intrusions will be observed.

Perhaps the major limitation on developing a mechanism for staircase formation in the Arctic Ocean has been considered to relate to the fact that the magnitude of the observed vertical density ratio ($\bar{R}_\rho \sim 4$; see, e.g., Timmermans et al. 2008) falls outside the DC-unstable range ($1 < \bar{R}_\rho < 1.1$) derived by linear stability analysis of the Boussinesq equations (Veronis 1965). However, this derivation considers only small-scale dynamics (i.e., molecular diffusivities are used in the computation of fluxes), and no horizontal background gradients in temperature and salinity. Here, we invoke the parametric flux model [as used by Merryfield (2000) for the SF case] to determine a critical vertical density ratio \bar{R}_ρ^{cr} for the DC stratification at which a transition between staircases and intrusions occurs for the observed vertical and lateral temperature gradients in the Arctic Ocean. In this formalism, instability does not require \bar{R}_ρ to be less than 1.1.

The paper is organized as follows: In the next section, we formulate the governing equations (section 2a) and then determine a constraint on the growth rate for growing perturbations to evolve toward a DC staircase (section 2b). Next, in section 2c, we perform a linear stability analysis on the governing Boussinesq equations to determine the fastest-growing mode as a function of vertical and lateral temperature and salinity gradients. Together with the result from section 2b, this allows us to define a critical vertical density ratio \bar{R}_ρ^{cr} above which intrusions form and below which staircases form. In section 3, we introduce Ice-Tethered Profiler (ITP; Krishfield et al. 2008; Toole et al. 2011) measurements of temperature and salinity through the Canada Basin double-diffusive thermocline, which features both a staircase and intrusions. We show that ITP measurements are consistent with the theory for reasonable estimates of appropriate parameters. Findings are summarized and discussed in section 4.

2. Theory

a. Formulation of the governing equations

We begin by formulating the governing equations accounting for three scales of motion as described in section 1. The governing set of Boussinesq equations (2D; horizontal and vertical dimensions) is as follows:

$$\begin{aligned}
 u_t + uu_x + wu_z &= -p_x/\rho_0 + \nu \nabla^2 u, \\
 w_t + uw_x + ww_z &= -p_z/\rho_0 - g\rho/\rho_0 + \nu \nabla^2 w, \\
 u_x + w_z &= 0, \\
 T_t + uT_x + wT_z &= \kappa_T \nabla^2 T, \\
 S_t + uS_x + wS_z &= \kappa_S \nabla^2 S, \quad \text{and} \\
 \rho &= \rho(T, S),
 \end{aligned} \tag{1}$$

where u and w are horizontal and vertical components of velocity; p is pressure; κ_T and κ_S are the molecular coefficients of heat and salt diffusion, respectively; and ν is the molecular kinematic viscosity. We neglect rotation because we are primarily interested in the fastest growth rate; with respect to the SF case, [Kerr and Holyer \(1986\)](#) have shown that the structure of the fastest-growing mode of perturbation (i.e., vertical and horizontal wavenumbers along with the growth rate) is unaffected by rotation. This set of equations consists of two momentum equations, the continuity equation, conservation equations for T and S , and the equation of state of seawater.

We proceed by decomposing variables into large-scale values (basinwide scales, denoted by overbars), medium scales (intrusions, denoted by tildes), and small scales (double-diffusive mixing, denoted by primes), for example, $u = \bar{u} + \tilde{u} + u'$, $T = \bar{T} + \tilde{T} + T'$, and so on ([Stern 1967](#)); this is similar to the separation of scales under Reynolds averaging ([Reynolds 1894](#)). All equations are next averaged over small scales associated with double-diffusive mixing on a time period that is sufficiently long to smooth transient fluctuations, yet short enough to retain the slow evolution of the interleaving motion (operating on medium scales). Further, we assume that the background state is motionless (i.e., $\bar{u} = 0$ and $\bar{w} = 0$). Note also that the background temperature and salinity structure do not change on the time scales of medium motion, so that $\partial\bar{T}/\partial t = 0$ and $\partial\bar{S}/\partial t = 0$; in [section 3b](#), we show this to be an appropriate approximation for the setting considered here. After time averaging (denoted by angle brackets, and note that time averaging of any medium- or large-scale variable is equal to that variable; e.g., $\langle \tilde{u} \rangle = \tilde{u}$), the governing equations become

$$\begin{aligned}
 \tilde{u}_t + \tilde{u}\tilde{u}_x + \tilde{w}\tilde{u}_z &= -\tilde{p}_x/\rho_0 + \nu\nabla^2\tilde{u} - (\langle u'u' \rangle)_x - (\langle u'w' \rangle)_z, \\
 \tilde{w}_t + \tilde{u}\tilde{w}_x + \tilde{w}\tilde{w}_z &= -\tilde{p}_z/\rho_0 - g\tilde{\rho}/\rho_0 + \nu\nabla^2\tilde{w} - (\langle u'w' \rangle)_x \\
 &\quad - (\langle w'w' \rangle)_z, \\
 \tilde{u}_x + \tilde{w}_z &= 0, \\
 \tilde{T}_t + \tilde{u}\tilde{T}_x + \tilde{w}\tilde{T}_z + \tilde{u}\bar{T}_x + \tilde{w}\bar{T}_z \\
 &= \kappa_T\nabla^2(\bar{T} + \tilde{T}) - (\langle u'T' \rangle)_x - (\langle w'T' \rangle)_z, \quad \text{and} \\
 \tilde{S}_t + \tilde{u}\tilde{S}_x + \tilde{w}\tilde{S}_z + \tilde{u}\bar{S}_x + \tilde{w}\bar{S}_z \\
 &= \kappa_S\nabla^2(\bar{S} + \tilde{S}) - (\langle u'S' \rangle)_x - (\langle w'S' \rangle)_z.
 \end{aligned} \tag{2}$$

The last two terms (Reynolds stresses) on the right-hand side of the two momentum, heat, and salt equations represent the effects of fluctuations (associated with double-diffusive mixing) on interleaving motions.

Horizontal flux divergences can be neglected with respect to vertical flux divergences since interleaving motions have small aspect ratio (e.g., [Walsh and Ruddick 1995](#)).

Analogous to Reynolds averaging, we combine Reynolds stresses and frictional terms to define vertical eddy viscosity A and vertical eddy diffusivities for heat K_T and salt K_S as follows:

$$\nu\tilde{u}_z - \langle u'w' \rangle = A\tilde{u}_z, \tag{3}$$

$$\nu\tilde{w}_z - \langle w'w' \rangle = A\tilde{w}_z, \tag{4}$$

$$\kappa_T(\bar{T} + \tilde{T})_z - \langle w'T' \rangle = K_T(\bar{T} + \tilde{T})_z, \quad \text{and} \tag{5}$$

$$\kappa_S(\bar{S} + \tilde{S})_z - \langle w'S' \rangle = K_S(\bar{S} + \tilde{S})_z. \tag{6}$$

The resulting linearized system of equations describes motions on the medium scale:

$$\tilde{u}_t + \tilde{p}_x/\rho_0 + F_z^u = 0, \tag{7}$$

$$\tilde{w}_t + \tilde{p}_z/\rho_0 + g\tilde{\rho}/\rho_0 + F_z^w = 0, \tag{8}$$

$$\tilde{u}_x + \tilde{w}_z = 0, \tag{9}$$

$$\tilde{T}_t + \tilde{u}\bar{T}_x + \tilde{w}\bar{T}_z + F_z^T = 0, \quad \text{and} \tag{10}$$

$$\tilde{S}_t + \tilde{u}\bar{S}_x + \tilde{w}\bar{S}_z + F_z^S = 0, \tag{11}$$

where vertical fluxes of horizontal F^u and vertical F^w momentum as well as vertical fluxes of heat F^T and salt F^S are defined as

$$F^u = -A\tilde{u}_z, \quad F^w = -A\tilde{w}_z, \quad \text{and} \tag{12}$$

$$F^T = -K_T(\bar{T} + \tilde{T})_z, \quad F^S = -K_S(\bar{S} + \tilde{S})_z. \tag{13}$$

The salt flux may be expressed via F^T and the ratio of the density flux of salt to the density flux of heat (i.e., the flux ratio $R_F = \beta F^S/\alpha F^T$) as

$$F^S = R_F \frac{\alpha}{\beta} F^T. \tag{14}$$

For the DC type of double-diffusive convection, it has been shown experimentally that $R_F \approx 0.15$ when $\bar{R}_\rho \geq 2$ ([Turner 1965](#)). Here, we take $R_F = 0.15$ for the medium-scale motions under the assumption that fluxes on medium scales can be parameterized as double-diffusive mixing on medium scales (see [Stern 1967](#)) and that the DC fluxes dominate [cf. [Toole and Georgi \(1981\)](#) and [Walsh and Ruddick \(1995, 2000\)](#) who followed the same reasoning for the SF case].

ESTIMATES OF K_T AND A

In the staircase region K_T may be estimated using a double-diffusive heat flux parameterization based on a 4/3 flux law ([Kelley 1990](#)), which uses the temperature

difference across an interface between two adjacent mixed layers and the bulk vertical temperature gradient; Guthrie et al. (2015) show the 4/3 flux law to be a reasonable representation of the fluxes. This yields $K_T = O(10^{-6}) \text{ m}^2 \text{ s}^{-1}$ for typical double-diffusive fluxes in the Canada Basin around $0.1\text{--}0.2 \text{ W m}^{-2}$ (Padman and Dillon 1987; Timmermans et al. 2008). This estimate for K_T is consistent with microstructure estimates by Guthrie et al. (2013) in the Canada Basin in the region of the staircase, where they find $K_T = 1\text{--}5 \times 10^{-6} \text{ m}^2 \text{ s}^{-1}$.

Eddy viscosity must be formulated to represent momentum transfer on medium scales due to double-diffusive processes. We begin with the turbulent kinetic energy balance

$$P_k + b - \varepsilon = 0, \tag{15}$$

where P_k is shear production, b is buoyancy production, and ε is the rate of viscous dissipation (e.g., Gregg 1987). In our theoretical framework, we consider growing perturbations in the absence of large-scale background shear ($P_k = 0$). As perturbations grow, however, small velocities arise associated with interleaving. We consider the intrusions here similar to a plume framework; the only shear in the system is that which arises as driven by buoyancy fluxes. The rate of dissipation of turbulent kinetic energy through viscosity can be parameterized in terms of this medium-scale shear and eddy viscosity as $\varepsilon = A\tilde{u}_z^2$. Thus, interleaving motions achieve a buoyancy production–viscous dissipation balance [see (15)] sometime after the onset of perturbations (see also McDougall 1985). Eddy viscosity can then be determined as follows:

$$A\tilde{u}_z^2 = g\alpha F^T(1 - R_F) \Rightarrow A \approx \frac{g\alpha K_T \bar{T}_z(1 - R_F)H^2}{U_0^2},$$

where \tilde{u}_z is scaled as U_0/H and typical interleaving velocity along a layer [of characteristic height $H = O(1) \text{ m}$] is $U_0 = O(1) \text{ mm s}^{-1}$ (Ruddick and Hebert 1988; Walsh and Carmack 2003). This yields $A = O(10^{-7}\text{--}10^{-6}) \text{ m}^2 \text{ s}^{-1}$ over the depth range $\sim 260\text{--}360 \text{ m}$ with the smaller values closer to the AW temperature maximum where \bar{T}_z is smaller. These estimates give the effective Prandtl number $\sigma = A/K_T$, ranging from $O(1)$ at shallow depths to $O(0.1)$ at deeper depths. These values are in general agreement with previous studies; for example, Padman (1994) estimates σ for the Canada Basin staircase to be between 1 and 3, albeit in the presence of weak large-scale background shear.

b. Constraint leading to a staircase

To derive a constraint on the growth rate that must be satisfied for a perturbation to evolve to a staircase, we

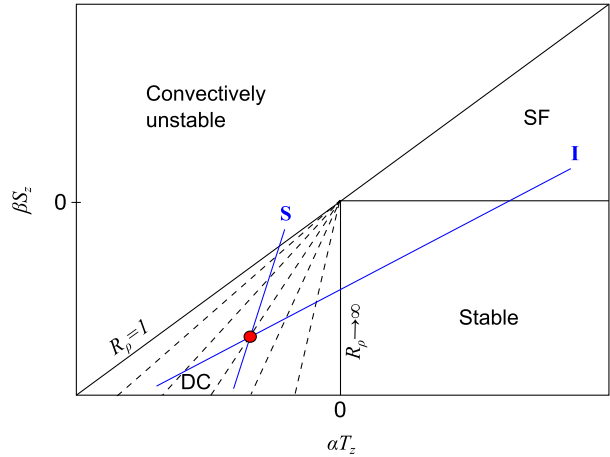


FIG. 2. Schematic showing evolution of temperature and salinity according to (16) and (17) (following Merryfield 2002). Dashed lines are constant R_p contours, bounded by two solid lines where $R_p = 1$ and $R_p \rightarrow \infty$. Blue lines show evolution of the initial perturbation from a background state (red dot, characterized by R_p) toward either a staircase S or intrusions I. There are four regimes shown on the diagram depending upon values of $(\alpha T_z, \beta S_z)$: DC-unstable, convectively unstable, SF-unstable, and stable stratification.

consider wavelike solutions of the system (7)–(11). We write temperature and salinity fields as the sum of linear background gradients plus deviations (resulting from interleaving motions) in the form of a plane wave, as follows:

$$T(x, z, t) = \bar{T}_z z + \bar{T}_x x + \tilde{T} = \bar{T}_z z + \bar{T}_x x + \mathbb{T}e^{ikx+imz+\lambda t}, \tag{16}$$

and

$$S(x, z, t) = \bar{S}_z z + \bar{S}_x x + \tilde{S} = \bar{S}_z z + \bar{S}_x x + \mathbb{S}e^{ikx+imz+\lambda t}, \tag{17}$$

where k and m are horizontal and vertical wave-numbers, respectively; λ is the growth rate; and \mathbb{T} and \mathbb{S} are the amplitudes of the temperature and salinity perturbations. Merryfield (2000) provides an effective explanation for the possible outcomes of a perturbation, given the initial conditions of an SF stratification; we follow the same reasoning for the DC case. At a particular $x = x_0$, the evolution of temperature and salinity can be illustrated on the $(\alpha T_z, \beta S_z)$ plane (Fig. 2). At time $t = 0$, the system is unperturbed and vertical gradients take the constant values $T_z(x_0, z, 0) = \bar{T}_z$ and $S_z(x_0, z, 0) = \bar{S}_z$. That is, the T and S fields are represented by a single point on the plane. After finite time t , the perturbed temperature and salinity fields may be written as

$$T_z(x_0, z, t) = \overline{T}_z + im\mathbb{T}e^{ikx_0+imz+\lambda t}, \quad \text{and}$$

$$S_z(x_0, z, t) = \overline{S}_z + imS_e e^{ikx_0+imz+\lambda t}.$$

Thus, a growing perturbation may be represented on the plane as a line segment with slope

$$\frac{\beta[S_z(x_0, z, t) - S_z(x_0, z, 0)]}{\alpha[T_z(x_0, z, t) - T_z(x_0, z, 0)]} = \frac{\beta S}{\alpha \mathbb{T}}.$$

If this slope is smaller than the vertical density ratio \overline{R}_ρ , characterizing the background stratification (i.e., large scale) from which a perturbation begins to grow, then the value of $\beta\tilde{S}_z/\alpha\tilde{T}_z$ increases in time on one end of the segment and decreases on the other end (Fig. 2, line denoted I for intrusion). An increase of $\beta\tilde{S}_z/\alpha\tilde{T}_z$ leads to a doubly stable stratification (i.e., the vertical temperature gradient reverses sign to decreasing temperature with depth, while the salinity gradient remains stable), with further increases leading to an SF-unstable stratification when the salinity gradient also reverses sign. The other end of the line segment I represents DC-favorable conditions with decreasing $\beta\tilde{S}_z/\alpha\tilde{T}_z$ toward unity, where convective instability takes place and a mixed layer is formed. Therefore, the evolution along line I corresponds to the development of intrusions consisting of alternating mixed layers, DC gradients, stable regions, and SF gradients. The second scenario (depicted by the line S for staircase in Fig. 2) arises when the evolution of T and S gradients are on a slope that is larger than \overline{R}_ρ . In this scenario, as the perturbation grows, $\beta\tilde{S}_z/\alpha\tilde{T}_z$ decreases on one end of the segment (toward $\beta\tilde{S}_z/\alpha\tilde{T}_z = 1$ and the convectively unstable region) and increases on the other end of the segment in the DC-unstable region of the $(\alpha T_z, \beta S_z)$ plane (Fig. 2, S). The growing perturbations result in a series of convectively unstable mixed layers and DC gradients, that is, a DC-type staircase. Whether a perturbation evolves to intrusions (along line I) or to a DC staircase (along line S) depends upon the growth rate and wavelengths of the perturbations, a function of the initial background temperature and salinity gradients. The explicit assumption here is that the evolution of temperature and salinity is in the linear phase (i.e., perturbations develop and grow exponentially and retain the same plane wave spatial dependence as they grow from infinitesimally small perturbations).

We begin by examining the case in which perturbations to the linear background gradient evolve into a staircase, that is,

$$\frac{\beta S}{\alpha \mathbb{T}} > \overline{R}_\rho. \quad (18)$$

Combining (10)–(11) and (16)–(18) and introducing a streamfunction $\tilde{\psi} = \Psi e^{ikx+imz+\lambda t}$ (where Ψ is the amplitude), such that

$$\tilde{\psi}_x = \tilde{w}, \quad \tilde{\psi}_z = -\tilde{u}, \quad (19)$$

we obtain the following criterion that the growth rate λ must satisfy,

$$\lambda < \frac{m^2 K_T}{\overline{R}_\rho - 1} \left[1 - R_F - \frac{s}{\Gamma} (\overline{R}_\rho - R_F) \right], \quad (20)$$

in order for a perturbation to evolve to a staircase [from criterion (18)]. Here, $\Gamma = \overline{T}_x/\overline{T}_z$ and $s = k/m$ (the slope of the growing perturbations). We have assumed that the aspect ratio of the background state is always larger than the aspect ratio of the perturbations [i.e., $\Gamma/(\Gamma - s) > 0$], which is always satisfied for the observed values of \overline{T}_x and \overline{T}_z .

We next perform a linear stability analysis (see, e.g., Toole and Georgi 1981; Walsh and Ruddick 1995, 2000) on the system (7)–(11) to compute the most unstable mode (i.e., maximal λ and corresponding k and m) for a specified \overline{T}_x , \overline{T}_z , and \overline{R}_ρ . The result is used together with the condition (20) to derive a critical density ratio $\overline{R}_\rho^{\text{cr}}$ below which staircases are expected to be the end result of an interleaving perturbation.

c. Critical density ratio

To reduce the number of equations in the system, we combine (7)–(9) (plus the seawater equation of state) to yield an evolution equation for vorticity $\nabla^2 \tilde{\psi}$:

$$\nabla^2 \tilde{\psi}_t + g(\beta\tilde{S}_x - \alpha\tilde{T}_x) + F_{xz}^w - F_{zz}^u = 0. \quad (21)$$

Multiplying (10) by α and (11) by β , and substituting for the fluxes [(12)–(14)], the final system of equations can be expressed as

$$\nabla^2 \tilde{\psi}_t + g(\beta\tilde{S}_x - \alpha\tilde{T}_x) - A\nabla^2 \tilde{\psi}_{zz} = 0, \quad (22)$$

$$\alpha\tilde{T}_t - \tilde{\psi}_z \alpha\overline{T}_x + \tilde{\psi}_x \alpha\overline{T}_z - \alpha K_T \tilde{T}_{zz} = 0, \quad \text{and} \quad (23)$$

$$\beta\tilde{S}_t - \tilde{\psi}_z \alpha\overline{T}_x + \tilde{\psi}_x \overline{R}_\rho \alpha\overline{T}_z - R_F \alpha K_T \tilde{T}_{zz} = 0. \quad (24)$$

In these equations, we have further made the assumption that horizontal background gradients in temperature and salinity are density compensating such that $\alpha\overline{T}_x = \beta\overline{S}_x$. This is appropriate with respect to the Arctic observations to be considered here; isopycnals are effectively parallel to isobars at depths where double diffusion is active. This assumption and the definition of \overline{R}_ρ allows background salinity gradients to be expressed in terms of background temperature gradients as

$$\overline{S}_x = \alpha \overline{T}_x / \beta, \quad \text{and} \quad (25)$$

$$\overline{S}_z = \overline{R}_\rho \alpha \overline{T}_z / \beta. \quad (26)$$

Again assuming plane wave solutions for the medium-scale motions $(\psi, \tilde{T}, \tilde{S}) = (\Psi, \mathbb{T}, \mathbb{S})e^{ikx+imz+\lambda t}$, the system [(22)–(24)] reduces to

$$\begin{bmatrix} -(k^2 + m^2)(Am^2 + \lambda) & -igk & igk \\ i\alpha(k\overline{T}_z - m\overline{T}_x) & \lambda + K_T m^2 & 0 \\ i\alpha(R_\rho k\overline{T}_z - m\overline{T}_x) & R_F K_T m^2 & \lambda \end{bmatrix} \begin{pmatrix} \Psi \\ \alpha\mathbb{T} \\ \beta\mathbb{S} \end{pmatrix} = 0.$$

A solution to this exists only if the determinant of the coefficient matrix is equal to zero, which gives

$$\begin{aligned} &\lambda^3 m^2 (s^2 + 1) + \lambda^2 m^4 (A + K_T) (s^2 + 1) \\ &+ \lambda [AK_T m^6 (s^2 + 1) + \alpha \overline{T}_z g s^2 m^2 (1 - \overline{R}_\rho)] \\ &+ \alpha K_T g m^4 s [\overline{T}_x (1 - R_F) - \overline{T}_z s (\overline{R}_\rho - R_F)] = 0. \end{aligned} \quad (27)$$

The growth rate λ_{\max} of the fastest-growing mode (and corresponding values s_{\max} and m_{\max}) can be determined from (27) by applying a constrained optimization technique using the method of Lagrange multipliers (Bertsekas 2014) for a given \overline{T}_x and \overline{T}_z . We wish to maximize the growth rate λ , which may be expressed as a function of three variables $f(\lambda, m, s) = \lambda$ subject to the constraint given by (27), which we denote as $G(\lambda, m, s) = 0$. In the method of Lagrange multipliers, we construct a system of equations that satisfy $\nabla f(\lambda, m, s) = a \nabla G(\lambda, m, s)$ (where a is a constant), subject to $G(\lambda, m, s) = 0$. This yields four equations and four unknowns. Next, using solutions of the system (i.e., $\lambda_{\max}, m_{\max}, s_{\max}$) we can obtain $\overline{R}_\rho^{\text{cr}}$ from the criterion (20). That is, we solve the following equation:

$$\frac{\lambda_{\max}}{m_{\max}^2} = \frac{K_T}{\overline{R}_\rho^{\text{cr}} - 1} \left[1 - R_F - \frac{s}{\Gamma} (\overline{R}_\rho^{\text{cr}} - R_F) \right]. \quad (28)$$

In sum, we take the following steps to compute $\overline{R}_\rho^{\text{cr}}$: 1) estimate background lateral and vertical gradients; 2) use these in (27) to determine the most unstable growth rate λ_{\max} (and corresponding wavenumbers m_{\max} and k_{\max}) by employing a constrained optimization technique; and 3) use λ_{\max}, k_{\max} , and m_{\max} , as well as our estimates of K_T and R_F , to compute $\overline{R}_\rho^{\text{cr}}$ from (28).

3. Context with ITP observations

As a consistency check, we aim to examine whether the presence of intrusions or staircases in the Arctic

Ocean water column is commensurate with the linear theory described in the previous section. Given the significant uncertainty in system parameters, as well as nonlinear effects, we do not assert that the formalism may be used in a predictive capacity. Rather, the motivation for exploring the observations in context with the linear theory is to provide some physical intuition for the physics of staircases and intrusions in the Arctic setting. Water column measurements are from an ITP (Krishfield et al. 2008; Toole et al. 2011) that drifted in the Canada Basin (Fig. 1). ITPs are automated profiling instruments that provide measurements of temperature, salinity, and depth from several meters depth beneath the sea ice, through the Atlantic Water layer to about 750-m depth. The final processed data for ITP system number 2 (ITP 2), operating between August 2004 and September 2004, are analyzed here. Measurements have a vertical resolution of about 25 cm and a horizontal profile spacing of a few kilometers; full processing procedures are given by Krishfield et al. (2008). ITP data have been analyzed in several past studies of double diffusion in the Canada Basin (e.g., Timmermans et al. 2008; Radko et al. 2014; Bebieva and Timmermans 2016; Shibley et al. 2017). We will examine ITP profiles to compare the observed vertical density ratio \overline{R}_ρ in depth regions exhibiting staircases and intrusions with the critical density ratio $\overline{R}_\rho^{\text{cr}}$ computed for the observed vertical and horizontal background gradients and \overline{R}_ρ .

a. Quantifying the temperature and salinity gradients

Before applying the theory, we require some method to assess the bulk temperature and salinity gradients ($\overline{T}_z, \overline{S}_z$ and $\overline{T}_x, \overline{S}_x$) in the ITP measurements.

1) VERTICAL GRADIENTS

To compute \overline{T}_z and \overline{S}_z (and therefore \overline{R}_ρ), we consider the depth range between a shallow bound of the AW layer (around 260-m depth) to the depth of the AW temperature maximum around 360-m depth. Vertical profiles of \overline{T}_z are constructed by performing a cubic spline with a smoothing parameter chosen to smooth the small and medium scales in the profiles while retaining the large-scale structure. The same technique is applied to estimate \overline{S}_z .

2) HORIZONTAL GRADIENTS

The drift track of the ITP is approximately from west to east, with some meandering (Fig. 1a); the horizontal distance between profiles varies (between around 2 and 7 km) with variations in sea ice drift speed. All measurements are projected onto 77°N (the x direction)

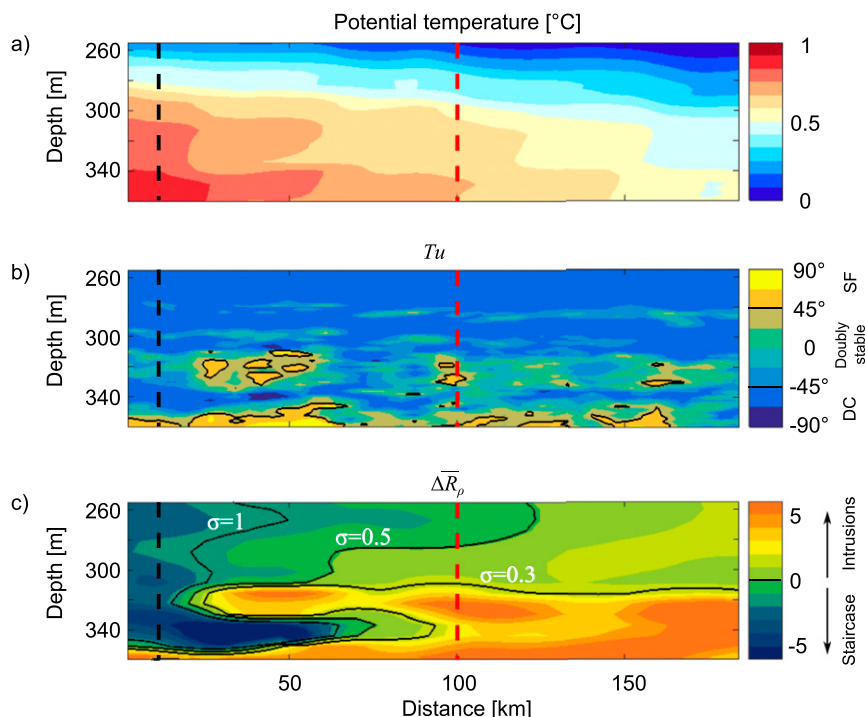


FIG. 3. Depth (m)–distance (km) section of (a) potential temperature ($^{\circ}\text{C}$, referenced to the surface). (b) Turner angle Tu (black contours indicate $Tu = 45^{\circ}$); Tu is calculated after first computing a 5-m running average of the full-resolution (~ 25 cm) T and S profiles. (c) $\Delta\bar{R}_{\rho}$ (see text) for $\sigma = 0.5$ (black contours indicate $\Delta\bar{R}_{\rho} = 0$ for $\sigma = 1, 0.5, 0.3$). Measurements correspond to the ITP drift track (Fig. 1a) projected onto 77°N (distance is positive east). Vertical dashed lines mark the locations of the west (black) and east (red) profiles shown in Figs. 1b and 1c.

and interpolated to a 4-km horizontal grid. The temperature is taken along isopycnals (effectively parallel to isobars) in the considered depth range (260–360 m), and the lateral background gradient \bar{T}_x is computed using a cubic spline fitting procedure with a spline parameter determined such that small and medium scales are removed while large-scale horizontal gradients are retained.

b. Comparison with theory

The basic temperature structure sampled by ITP 2 in the considered depth range is as follows: AW temperatures cool from west to east across the basin with stronger lateral gradients in the deeper portion of the depth range compared to the shallower portion (note that the considered depth range includes only the upper part of the AW layer where bulk temperature and salinity gradients are increasing with depth; Fig. 3a). At the depth ranges of interest, the water column structure is effectively unchanging in time over the sampling duration (~ 40 days) of the ITP as it drifted from west to east (Fig. 1a).

Detailed examination of the temperature and salinity profiles indicates that some regions exhibit only staircases throughout the considered depth range, while others show either a staircase overlying intrusions or alternating (in depth) staircases and intrusions (Figs. 1b–d). Note that several studies have exploited T – S space in examining these features because the properties of staircase layers and intrusions (Fig. 1d) tend to lie along well-defined regions in T – S space (see, e.g., Timmermans et al. 2008; Walsh and Carmack 2003). However, for our purposes here, we have found that the best metric to characterize the range of double-diffusive structures is the Turner angle $Tu = \tan^{-1}[(1 + R_{\rho})/(1 - R_{\rho})]$, which indicates the stability of a water column with respect to double-diffusive processes (Ruddick 1983). When a staircase is present, the water column is characterized by $-90^{\circ} < Tu < -45^{\circ}$. When intrusions are present, SF regions ($45^{\circ} < Tu < 90^{\circ}$) alternate in depth with DC regions ($-90^{\circ} < Tu < -45^{\circ}$). A doubly stable water column is characterized by $-45^{\circ} < Tu < 45^{\circ}$. The angle Tu is calculated after first computing a 5-m running average of the full-resolution (~ 25 cm) T and S profiles;

this averaging was chosen as a trade-off between the necessity for fine vertical resolution and elimination of noise in the profiles. Provided the running averaging is over depth intervals smaller than around 5 m, the general pattern of the Tu section, delineating where SF and DC regions are present, is insensitive to the choice of smoothing. The upper part of the AW layer (~ 260 – 300 m) consists predominantly of a staircase in the sampled region (Fig. 3b). Deeper than around 320-m depth, SF-unstable regions (indicative of intrusions) may be present. For example, in the west, we observe a staircase over most of the considered depth range; see also the western profile in Figs. 1b and 1c (black lines, with position indicated by the vertical black dashed line in Fig. 3b). In the eastern part of the section, we observe intrusions around 320 m and deeper; see also the eastern profile in Figs. 1b and 1c (red lines, with position indicated by the vertical red dashed line in Fig. 3b).

The quantities \overline{R}_ρ and $\overline{R}_\rho^{\text{cr}}$ are computed using the estimated background \overline{T}_z , \overline{S}_z , and \overline{T}_x sampled by the ITP (and specifying a reasonable value of σ , as estimated in section 2a). A staircase is expected where $\Delta\overline{R}_\rho = \overline{R}_\rho - \overline{R}_\rho^{\text{cr}} < 0$, while intrusions are expected where $\Delta\overline{R}_\rho > 0$. The transition between these two regimes corresponds to $\Delta\overline{R}_\rho = 0$, which is sensitive to variations in σ (Fig. 3c; this uncertainty is discussed further in section 4).

Our linear stability analysis together with (28) indicates that $\overline{R}_\rho^{\text{cr}}$ is relatively insensitive to variations in \overline{T}_x for some specified \overline{T}_z and \overline{S}_z [a similar result was found for the SF case; see the appendix in Merryfield (2000)]. Physically, this may be explained by the fact that the ratio of horizontal to vertical wavenumbers of the most unstable mode varies proportionally to the aspect ratio of the background temperature gradients. That is, $s_{\text{max}}/\Gamma = \text{const}$ (≈ 0.1 for the range of \overline{T}_x and \overline{T}_z here). It is also of interest to note that $\lambda_{\text{max}}/(K_T m_{\text{max}}^2)$ remains constant with varying \overline{T}_x , implying that the growth rate λ_{max} is always such that it is proportional to the diffusive time scale $1/(K_T m_{\text{max}}^2)$. While λ_{max} is faster for larger \overline{T}_x , this does not affect whether a staircase or intrusions are the end result of a perturbation to a linear background stratification. The main influencing parameters in this regard are \overline{T}_z and \overline{S}_z (and \overline{R}_ρ). For larger \overline{T}_z (e.g., at the westernmost part of the ITP sampling region, shallower than ~ 360 m; Fig. 3), it is more likely that $\Delta\overline{R}_\rho < 0$ (i.e., a staircase results from interleaving perturbations). In general, in the western part of the section, staircases are favored over most of the depth range. Farther to the east, $\Delta\overline{R}_\rho > 0$ indicates that intrusions may be present. This finding is consistent with the Tu characterization (Fig. 3b). It is important to emphasize that Tu was estimated using information that accounts for the finescale temperature and salinity features in the vertical, while

$\Delta\overline{R}_\rho$ was estimated by considering only the background (vertical and horizontal) gradients.

It is instructive to examine the characteristic time and length scales of the most unstable modes leading to either a staircase or intrusions. The horizontal and vertical wavelengths of the most unstable modes are of the order of 1000–10 000 km and 15–50 m, respectively, in the sampled region of the Canada Basin; vertical scales are generally consistent with scales of variability in staircase/intrusion regions of the Canada Basin. Similar scales of the most unstable modes leading to either a staircase or intrusions suggest that these two end states are of the same nature. Of course, the linear theory cannot predict the transient evolution of the linear profile [e.g., how interleaving motions evolve and the associated scale adjustments such as layer splitting/merging (Radko et al. 2014)]; this requires a separate analysis [as performed, e.g., by Walsh and Ruddick (1998) and Li and McDougall (2015) for the SF case]. The time scale of the instability (determined from the fastest-growing mode) ranges from several months to about a year for both intrusions and a staircase and depends on the magnitude of the horizontal temperature gradient (with shorter time scales for larger \overline{T}_x).

Within our analysis is the implicit assumption that the development of intrusions or a staircase does not affect the magnitudes of the background gradient (i.e., that the background gradients do not evolve on time scales faster than the fastest-growing mode). An order-of-magnitude estimate for the time scale on which double-diffusive fluxes modify the background temperature gradients can be estimated as D^2/K_T , where D is a characteristic length scale for the background gradient. Taking $D \sim 30$ m for a vertical scale (a reasonable estimate over which linear gradients remain constant) and eddy diffusivity $K_T = 10^{-6} \text{ m}^2 \text{ s}^{-1}$ yields time scales of decades for modification of the vertical background temperature gradient. Similarly, considering a vertical eddy diffusivity for salinity of around $10^{-7} \text{ m}^2 \text{ s}^{-1}$ (e.g., Bebieva and Timmermans 2016), we find time scales for modification of the vertical background salinity gradient to be an order of magnitude longer than this. Following the same reasoning for the evolution of the lateral gradients [over $O(50$ – $100)$ km horizontal scales] and taking isopycnal diffusivities in the range 5 – $50 \text{ m}^2 \text{ s}^{-1}$ (Hebert et al. 1990; Walsh and Carmack 2003) also yield time scales of decades for the lateral gradients to evolve. Comparison of these time scale estimates to the maximal growth rates found here (i.e., several months to a year) suggests background gradients do not evolve on time scales shorter than those associated with the development of a perturbation toward either a staircase or intrusions; thus, in this

analysis, the background gradients may be approximated as independent of time.

4. Summary and discussion

We have examined a scenario for the origin of double-diffusive staircases and intrusions that are observed to coexist in the Arctic Ocean's AW. A linear stability analysis of the governing equations was performed to determine the most unstable mode for a given horizontal and vertical linear temperature and salinity stratification that would lead toward either staircases or intrusions. Staircases are the end result of a perturbation if the observed vertical density ratio is below a critical vertical density ratio ($\overline{R}_\rho < \overline{R}_\rho^{\text{cr}}$), and intrusions are expected to form otherwise ($\overline{R}_\rho > \overline{R}_\rho^{\text{cr}}$). The poor constraints on eddy diffusivity and viscosity preclude any predictive capacity for our formalism; for example, over possible ranges for A (10^{-7} – 10^{-6} $\text{m}^2 \text{s}^{-1}$) and K_T (10^{-6} – 10^{-5} $\text{m}^2 \text{s}^{-1}$), $\overline{R}_\rho^{\text{cr}}$ varies by a factor of 2. Nevertheless, comparison of our theoretical formalism to observations serves as a consistency assertion, and we have shown that the linear theory is consistent with the observations for reasonable estimates of A and K_T . Future analyses are required to explore the parameter space further, either numerically or in a laboratory setting.

We have shown that the dominant factors that determine the presence of either a staircase or intrusions are \overline{T}_z , \overline{S}_z , and \overline{R}_ρ , with lateral temperature gradients having little influence. In general, we expect staircases in regions of relatively strong \overline{T}_z (and small \overline{R}_ρ) and intrusions where \overline{T}_z is weaker. Consider, for example, an influx of warm AW in the water column. This would give rise to a stronger \overline{T}_z at the top boundary of the AW and a weaker \overline{T}_z above and close to the AW temperature maximum (i.e., within an approximately homogeneous core). Such a modification of the background state would result in the formation of staircases at the AW top boundary and intrusions in the underlying portions. This stratification allows for vertical as well as lateral heat transfer via the intrusions. If over time the background temperature gradient in the deeper portion increases, this new \overline{T}_z may be susceptible to formation of a staircase. One potential mechanism for increased \overline{T}_z could be that intrusions distribute heat more effectively downward via SF fluxes rather than upward via DC fluxes [e.g., see heat flux estimates in [Bebieva and Timmermans \(2016\)](#)], although the overall effect of intrusive fluxes on the background gradient is unclear. Formation of a staircase in place of intrusions would lead to reduced lateral transport of heat, and vertical fluxes would dominate heat transfer. In this respect, the lateral and vertical transfer of AW heat in the Arctic

Ocean is dictated by the interplay between time scales for intrusive fluxes to modify the background gradients and the lateral supply of AW heat. Further investigation is required to quantify these time scales.

For the SF configuration, [Merryfield \(2000\)](#) showed that staircases are the end result of a perturbation when the vertical density ratio (defined in the conventional way for the SF configuration, inverse to the definition given here) is small, while intrusions are the end state when that density ratio takes larger values. We have used the same formalism here to demonstrate that an analogous result is applicable to the DC case. That is, a staircase is a possible end state of an interleaving perturbation. [Merryfield \(2000\)](#) showed that a staircase is more likely for smaller values of the eddy diffusivity for salt. By contrast, we have shown that (for the DC configuration) a staircase is more likely for larger values of eddy diffusivity for heat K_T (i.e., smaller σ), although the physics of these relationships needs to be explained.

While the linear stability analysis and separation of scales framework described here may be instructive for understanding the general structure of a water column profile (i.e., staircases or intrusions), the Arctic Ocean observations often demonstrate a detailed finestructure that is somewhat more complicated (e.g., [Padman and Dillon 1989](#)). Our analysis cannot describe layers that are observed between and within the main staircase mixed layers and intrusive structures. These features, however, may be key to the transition between interleaving structures and staircases—a conjecture that will require further analysis.

Acknowledgments. The Ice-Tethered Profiler data were collected and made available by the Ice-Tethered Profiler Program based at the Woods Hole Oceanographic Institution ([Krishfield et al. 2008](#); [Toole et al. 2011](#)); data are available online (at <http://www.whoi.edu/itp/data>). Funding was provided by the National Science Foundation Division of Polar Programs under Award Number 1350046.

REFERENCES

- Aagaard, K., L. Coachman, and E. Carmack, 1981: On the halocline of the Arctic Ocean. *Deep-Sea Res.*, **28A**, 529–545, doi:10.1016/0198-0149(81)90115-1.
- Bebieva, Y., and M.-L. Timmermans, 2016: An examination of double-diffusive processes in a mesoscale eddy in the Arctic Ocean. *J. Geophys. Res. Oceans*, **121**, 457–475, doi:10.1002/2015JC011105.
- Bertsekas, D. P., 2014: *Constrained Optimization and Lagrange Multiplier Methods*. Academic Press, 344 pp.
- Carmack, E. C., K. Aagaard, J. H. Swift, R. G. Perkin, F. A. McLaughlin, R. W. Macdonald, and E. P. Jones, 1998: Thermohaline transitions. *Physical Processes in Lakes and Oceans*,

- J. Imberger, Ed., Coastal and Estuarine Studies, Vol. 54, Amer. Geophys. Union, 179–186.
- , and Coauthors, 2015: Toward quantifying the increasing role of oceanic heat in sea ice loss in the new Arctic. *Bull. Amer. Meteor. Soc.*, **96**, 2079–2105, doi:10.1175/BAMS-D-13-00177.1.
- Gregg, M., 1987: Diapycnal mixing in the thermocline: A review. *J. Geophys. Res.*, **92**, 5249–5286, doi:10.1029/JC092iC05p05249.
- Guthrie, J. D., J. H. Morison, and I. Fer, 2013: Revisiting internal waves and mixing in the Arctic Ocean. *J. Geophys. Res. Oceans*, **118**, 3966–3977, doi:10.1002/jgrc.20294.
- , I. Fer, and J. Morison, 2015: Observational validation of the diffusive convection flux laws in the Amundsen Basin, Arctic Ocean. *J. Geophys. Res. Oceans*, **120**, 7880–7896, doi:10.1002/2015JC010884.
- Hebert, D., N. Oakey, and B. Ruddick, 1990: Evolution of a Mediterranean salt lens: Scalar properties. *J. Phys. Oceanogr.*, **20**, 1468–1483, doi:10.1175/1520-0485(1990)020<1468:EOAMSL>2.0.CO;2.
- Kelley, D. E., 1990: Fluxes through diffusive staircases: A new formulation. *J. Geophys. Res.*, **95**, 3365–3371, doi:10.1029/JC095iC03p03365.
- , 2001: Six questions about double-diffusive convection. *From Stirring to Mixing in a Stratified Ocean: Proc. 'Aha Huliko'a Hawaiian Winter Workshop*, Honolulu, HI, University of Hawai'i at Mānoa, 191–198. [Available online at <http://www.soest.hawaii.edu/PubServices/2001pdfs/Kelley.pdf>.]
- , H. Fernando, A. Gargett, J. Tanny, and E. Özsoy, 2003: The diffusive regime of double-diffusive convection. *Prog. Oceanogr.*, **56**, 461–481, doi:10.1016/S0079-6611(03)00026-0.
- Kerr, O. S., and J. Y. Holyer, 1986: The effect of rotation on double-diffusive interleaving. *J. Fluid Mech.*, **162**, 23–33, doi:10.1017/S0022112086001908.
- Krishfield, R., J. Toole, A. Proshutinsky, and M.-L. Timmermans, 2008: Automated Ice-Tethered Profilers for seawater observations under pack ice in all seasons. *J. Atmos. Oceanic Technol.*, **25**, 2091–2105, doi:10.1175/2008JTECHO587.1.
- Kunze, E., 2003: A review of oceanic salt-fingering theory. *Prog. Oceanogr.*, **56**, 399–417, doi:10.1016/S0079-6611(03)00027-2.
- Li, Y., and T. J. McDougall, 2015: Double-diffusive interleaving: Properties of the steady-state solution. *J. Phys. Oceanogr.*, **45**, 813–835, doi:10.1175/JPO-D-13-0236.1.
- Maykut, G. A., and N. Untersteiner, 1971: Some results from a time-dependent thermodynamic model of sea ice. *J. Geophys. Res.*, **76**, 1550–1575, doi:10.1029/JC076i006p01550.
- McDougall, T. J., 1985: Double-diffusive interleaving. Part II: Finite amplitude, steady state interleaving. *J. Phys. Oceanogr.*, **15**, 1542–1556, doi:10.1175/1520-0485(1985)015<1542:DDIPIF>2.0.CO;2.
- Melling, H., R. Lake, D. Topham, and D. Fissel, 1984: Oceanic thermal structure in the western Canadian Arctic. *Cont. Shelf Res.*, **3**, 233–258, doi:10.1016/0278-4343(84)90010-4.
- Merryfield, W. J., 2000: Origin of thermohaline staircases. *J. Phys. Oceanogr.*, **30**, 1046–1068, doi:10.1175/1520-0485(2000)030<1046:OOTS>2.0.CO;2.
- , 2002: Intrusions in double-diffusively stable Arctic waters: Evidence for differential mixing? *J. Phys. Oceanogr.*, **32**, 1452–1459, doi:10.1175/1520-0485(2002)032<1452:IIDDSA>2.0.CO;2.
- Neal, V. T., S. Neshyba, and W. Denner, 1969: Thermal stratification in the Arctic Ocean. *Science*, **166**, 373–374, doi:10.1126/science.166.3903.373.
- Padman, L., 1994: Momentum fluxes through sheared oceanic thermohaline steps. *J. Geophys. Res.*, **99**, 22 491–22 499, doi:10.1029/94JC01741.
- , and T. M. Dillon, 1987: Vertical heat fluxes through the Beaufort Sea thermohaline staircase. *J. Geophys. Res.*, **92**, 10 799–10 806, doi:10.1029/JC092iC10p10799.
- , and —, 1988: On the horizontal extent of the Canada Basin thermohaline steps. *J. Phys. Oceanogr.*, **18**, 1458–1462, doi:10.1175/1520-0485(1988)018<1458:OTHEOT>2.0.CO;2.
- , and —, 1989: Thermal microstructure and internal waves in the Canada Basin diffusive staircase. *Deep-Sea Res.*, **36A**, 531–542, doi:10.1016/0198-0149(89)90004-6.
- Perovich, D. K., J. A. Richter-Menge, K. F. Jones, and B. Light, 2008: Sunlight, water, and ice: Extreme Arctic sea ice melt during the summer of 2007. *Geophys. Res. Lett.*, **35**, L11501, doi:10.1029/2008GL034007.
- Polyakov, I. V., A. V. Pnyushkov, R. Rember, V. V. Ivanov, Y.-D. Lenn, L. Padman, and E. C. Carmack, 2012: Mooring-based observations of double-diffusive staircases over the Laptev Sea slope. *J. Phys. Oceanogr.*, **42**, 95–109, doi:10.1175/2011JPO4606.1.
- Radko, T., 2013: *Double-Diffusive Convection*. Cambridge University Press, 344 pp.
- , J. Flanagan, S. Stellmach, and M.-L. Timmermans, 2014: Double-diffusive recipes. Part II: Layer-merging events. *J. Phys. Oceanogr.*, **44**, 1285–1305, doi:10.1175/JPO-D-13-0156.1.
- Reynolds, O., 1894: On the dynamical theory of incompressible viscous fluids and the determination of the criterion. *Proc. Roy. Soc. London*, **56**, 40–45, doi:10.1098/rspl.1894.0075.
- Ruddick, B., 1983: A practical indicator of the stability of the water column to double-diffusive activity. *Deep-Sea Res.*, **30A**, 1105–1107, doi:10.1016/0198-0149(83)90063-8.
- , and D. Hebert, 1988: The mixing of meddy “Sharon.” *Small-Scale Turbulence and Mixing in the Ocean*, J. C. J. Nihoul and B. M. Jamart, Eds., Elsevier Oceanography Series, Vol. 46, 249–261, doi:10.1016/S0422-9894(88)70551-8.
- , and O. Kerr, 2003: Oceanic thermohaline intrusions: Theory. *Prog. Oceanogr.*, **56**, 483–497, doi:10.1016/S0079-6611(03)00029-6.
- , and K. Richards, 2003: Oceanic thermohaline intrusions: Observations. *Prog. Oceanogr.*, **56**, 499–527, doi:10.1016/S0079-6611(03)00028-4.
- Schmitt, R. W., 2003: Observational and laboratory insights into salt finger convection. *Prog. Oceanogr.*, **56**, 419–433, doi:10.1016/S0079-6611(03)00033-8.
- Shibley, N., M.-L. Timmermans, J. Carpenter, and J. Toole, 2017: Spatial variability of the Arctic Ocean's double-diffusive staircase. *J. Geophys. Res. Oceans*, **122**, 980–994, doi:10.1002/2016JC012419.
- Sirevaag, A., and I. Fer, 2012: Vertical heat transfer in the Arctic Ocean: The role of double-diffusive mixing. *J. Geophys. Res.*, **117**, C07010, doi:10.1029/2012JC007910.
- Steele, M., W. Ermold, and J. Zhang, 2008: Arctic Ocean surface warming trends over the past 100 years. *Geophys. Res. Lett.*, **35**, L02614, doi:10.1029/2007GL031651.
- Stern, M. E., 1967: Lateral mixing of water masses. *Deep-Sea Res. Oceanogr. Abstr.*, **14**, 747–753, doi:10.1016/S0011-7471(67)80011-1.
- Timmermans, M.-L., 2015: The impact of stored solar heat on Arctic sea ice growth. *Geophys. Res. Lett.*, **42**, 6399–6406, doi:10.1002/2015GL064541.
- , J. Toole, R. Krishfield, and P. Winsor, 2008: Ice-Tethered Profiler observations of the double-diffusive staircase in the Canada Basin thermocline. *J. Geophys. Res.*, **113**, C00A02, doi:10.1029/2008JC004829.
- , and Coauthors, 2014: Mechanisms of Pacific summer water variability in the Arctic's central Canada Basin.

- J. Geophys. Res. Oceans*, **119**, 7523–7548, doi:[10.1002/2014JC010273](https://doi.org/10.1002/2014JC010273).
- Toole, J. M., and D. T. Georgi, 1981: On the dynamics and effects of double-diffusively driven intrusions. *Prog. Oceanogr.*, **10**, 123–145, doi:[10.1016/0079-6611\(81\)90003-3](https://doi.org/10.1016/0079-6611(81)90003-3).
- , R. A. Krishfield, M.-L. Timmermans, and A. Proshutinsky, 2011: The Ice-Tethered Profiler: Argo of the Arctic. *Oceanography*, **24**, 126–135, doi:[10.5670/oceanog.2011.64](https://doi.org/10.5670/oceanog.2011.64).
- Turner, J., 1965: The coupled turbulent transports of salt and heat across a sharp density interface. *Int. J. Heat Mass Transfer*, **8**, 759–767, doi:[10.1016/0017-9310\(65\)90022-0](https://doi.org/10.1016/0017-9310(65)90022-0).
- Veronis, G., 1965: On finite amplitude instability in thermohaline convection. *J. Mar. Res.*, **23**, 1–17.
- Walsh, D., and B. Ruddick, 1995: Double-diffusive interleaving: The influence of nonconstant diffusivities. *J. Phys. Oceanogr.*, **25**, 348–358, doi:[10.1175/1520-0485\(1995\)025<0348:DDITIO>2.0.CO;2](https://doi.org/10.1175/1520-0485(1995)025<0348:DDITIO>2.0.CO;2).
- , and —, 1998: Nonlinear equilibration of thermohaline intrusions. *J. Phys. Oceanogr.*, **28**, 1043–1070, doi:[10.1175/1520-0485\(1998\)028<1043:NEOTI>2.0.CO;2](https://doi.org/10.1175/1520-0485(1998)028<1043:NEOTI>2.0.CO;2).
- , and —, 2000: Double-diffusive interleaving in the presence of turbulence: The effect of a nonconstant flux ratio. *J. Phys. Oceanogr.*, **30**, 2231–2245, doi:[10.1175/1520-0485\(2000\)030<2231:DDIITP>2.0.CO;2](https://doi.org/10.1175/1520-0485(2000)030<2231:DDIITP>2.0.CO;2).
- , and E. Carmack, 2003: The nested structure of Arctic thermohaline intrusions. *Ocean Modell.*, **5**, 267–289, doi:[10.1016/S1463-5003\(02\)00056-2](https://doi.org/10.1016/S1463-5003(02)00056-2).
- Wettlaufer, J., 1991: Heat flux at the ice-ocean interface. *J. Geophys. Res.*, **96**, 7215–7236, doi:[10.1029/90JC00081](https://doi.org/10.1029/90JC00081).
- Woodgate, R. A., K. Aagaard, J. H. Swift, W. M. Smethie, and K. K. Falkner, 2007: Atlantic water circulation over the Mendeleev Ridge and Chukchi Borderland from thermohaline intrusions and water mass properties. *J. Geophys. Res.*, **112**, C02005, doi:[10.1029/2005JC003416](https://doi.org/10.1029/2005JC003416).